Supporting Information

Quantifying transient interactions between *Bacillus* phosphatidylinositol-specific phospholipase-C and phosphatidylcholine-rich vesicles

Boqian Yang[1,2], Mingming Pu[2], Hanif M. Khan[3,4], Larry Friedman[5], Nathalie Reuter[3,4], Mary F. Roberts[2], Anne Gershenson[1*]

[1]Department of Biochemistry and Molecular Biology, University of Massachusetts, Amherst, MA U.S.A.; [2]Department of Chemistry, Boston College, Chestnut Hill, MA U.S.A; [3]Department of Molecular Biology and [4]Computational Biology Unit, University of Bergen, Bergen, Norway; [5]Department of Biochemistry, Brandeis University, Waltham, MA U.S.A.

Supporting Methods

Protein Expression and Purification

Recombinant *Bacillus thuringiensis* phosphatidylinositol-specific phospholipase C (*Bt*PI-PLC) containing the Asn168Cys (N168C) mutation for fluorescent labeling was expressed in *Escherichia coli* strain BL21-Codonplus(DE3)-RIL and purified as previously described.[1,2] The introduced Cys at residue 168 was labeled with Alexa Fluor 488 maleimide (AF488, Life Technologies) and the labeling efficiency was quantified according to the manufacturer's protocols. Labeling percentages were >90%. Labeling at residue 168 does not significantly affect BtPI-PLC specific activity or membrane binding.[2]

Preparation of Small Unilamellar Vesicles (SUVs)

SUVs were prepared by sonication as previously described.[2] SUV size distributions were determined using dynamic light scattering (DLS) on a Malvern Nano Zetasizer at the University of Massachusetts Amherst MRSEC (Materials Research Science & Engineering Center).

Fluorescence Correlation Spectroscopy (FCS) to Measure Binding

The affinity of AF488 labeled *Bt*PI-PLC for SUVs was determined using FCS.[2,3] In these experiments, 10 nM AF488 labeled *Bt*PI-PLC was titrated with increasing concentrations of SUVs and the apparent dissociation constants, K_ds, were determined as previously described.[2,3] To determine if addition of the lipophilic fluorophore DiD (Life Technologies) and the biotinylated dipalmitoyl phosphatidylethanolamine (biotin-PE, Avanti Polar Lipids) to the SUVs altered BtPI-PLC affinity, FCS experiments were performed using vesicles that containing 2 to 3% DiD and 1% biotin-PE. These experiments were conducted in parallel with FCS experiments using unlabeled (no DiD, no biotin-PE) vesicles, and no significant differences in the apparent K_ds were observed between labeled and unlabeled SUVs (Fig. S12).

The apparent K_ds in Figure 3 were determined from two independent experiments, and the uncertainties are the larger of (i) the standard deviations from two independent FCS experiments and (ii) the uncertainty generated by error propagation.

Sample Preparation for Total Internal Reflection Fluorescence (TIRF) Microscopy

To minimize fluorescence background, glass coverslips (Gold Seal) were cleaned by placing the coverslips in plastic, covered slide holders (Fisher Scientific, HS15986) containing the following solutions which were then placed in a sonicating water bath for the indicated amounts of time: (i) 2% micro-90 detergent sonicated for 1 h; (ii) 100% ethanol, sonicated for 1 h; (iii) 0.1 M KOH, sonicated for 30 min; (iv) MilliQ water, sonicated for approximately 10 min. Coverslips were extensively washed with water purified using a MilliQ system between cleaning steps. Cleaned coverslips were stored in 20% ethanol/water solutions for up to two weeks.

Before use, cleaned coverslips were sonicated in 0.1 KOH for approximately 15 min, followed by sonication in MilliQ water for about 5 min and extensive washing with MilliQ water. The coverslips were then thoroughly dried using nitrogen gas. Dried coverslips were aminosilanized by incubating in a 1% Vectabond (Vector Labs)-acetone solution for 5 min at room temperature. Silanized coverslips were rinsed in MilliQ water and dried. Prior to PEGylation, the longer of the two coverslips was divided into four lanes using silicon vacuum grease and the smaller coverslip was placed on top of the lanes. For PEGylation, solutions containing polyethylene glycol succinimidyl valerate (mPEG-SV, Laysan Bio) with an average molecular weight (MW) of 5000 Da and 1% biotin-PEG-SV, 5000 MW (Laysan Bio) in 0.1 M $NaHCO_3$ buffer, pH 8.3 were flowed into the lanes and allowed to incubate at room temperature for 2 to 3 h in a humidified home-made slide holder (hydration chamber) to avoid evaporation. These PEGylated slides were either used immediately or stored in the hydration chambers at 4° C for up to one week.

PEGylated slides were warmed up to room temperature as necessary and the lanes were extensively washed with phosphate buffered saline (PBS), pH 7.4. To immobilize fiduciary markers that could be observed in both channels for dual-color imaging, 40 nm diameter streptavidin-labeled fluorescent microspheres excitable at 488 nm and with a broad emission spectrum from 600 to 750 nm (Life Technologies, T10711) were diluted approximately 300,000 times, flowed into the lanes and allowed to incubate for 5 min after which free beads were removed by extensive washing with buffer. The bead concentration was high enough to immobilize on average 3 beads per field of view (Fig. S3). 0.01 mg/ml neutravidin (Life Technologies) in PBS, pH 7.4, was flowed into the lanes and incubated for 10 min to allow binding to the PEG-biotin, and excess neutravidin was removed by extensive washing with buffer. SUVs were immobilized on the PEG-biotin surface by flowing 20 μM of SUVs (containing 0.8 mole fraction 1-palmitoyl-2-oleoyl-phosphatidylcholine (POPC) (X_{PC}), 0.2 mole fraction dioleoylphosphatidylglycerol (DOPG), 2-3 mol% of the lipophilic fluorophore DiD and 1 mol% biotinylated dipalmitoyl phosphatidylethanolamine (biotin-PE)) in PBS, pH 7.4 into the lanes and incubating for 5 min at room temperature. Extensive washing with buffer removed SUVs that were not tethered to the surface. Just prior to performing vesicle binding experiments, 1 nM AF488 labeled *Bt*PI-PLC in PBS, pH 7.4, supplemented with the glucose oxidase/catalase/glucose deoxygenation system (0.2 mg/ml glucose oxidase (Sigma G-2133), 0.035mg/ml catalase (Sigma C-40), 4.5 mg/ml glucose (Sigma G-8270)) to prolong the photobleaching lifetimes[4,5] was flowed into the observed lane. To avoid pH changes due to the glucose oxidase/catalase deoxygenation system, *Bt*PI-PLC and the deoxygenation system were replaced every 10 to 15 minutes during the experiments by flowing in fresh solutions.

Single Molecule TIRF Microscopy

Single molecule TIRF experiments were performed at the NSF funded University of Massachusetts Amherst Single Molecule/Live Cell Imaging Facility. The microscope system is based on a Nikon Ti inverted microscope system with a purpose-built dual-view imaging system[6] containing an Andor iXon+

EMCCD camera. The dual-view contains two dichroic mirrors which split the fluorescence image by wavelength at 630 nm so that AF488 labeled *Bt*PI-PLC and the DiD labeled SUVs simultaneously appear in the <630 nm and >630 nm channels, respectively. Samples were excited at 488 nm (Melles Griot argon ion laser) and 647 nm (Diode Pumped Solid State laser (DPSS, Crystalaser)) using laser powers before the objective of 8 mW and 7.5 mW, respectively. The multi-color fluorescent beads serve as fiduciary marks that appear in both channels. The Nikon program Elements was used to control the microscope system and to collect data. The two-channel TIRF data were analyzed using Matlab (Mathworks). For more information on the image analysis see Figures 1, S2 and S3. To determine the effects of photobleaching, additional data were collected using 488 nm laser powers before the objective of 4 mW and 10 mW (Fig. S4).

Image Analysis

Image analysis included the following. (1) *Mapping:* Mapping files were generated using fluorescent beads. More than 1000 beads were selected to generate the correlation between areas of interest (AOIs) in the protein channel and AOIs in the vesicle channel. This correlation was then used to map vesicle locations in the vesicle channel onto the protein channel data; see Figure S2. (2) *Drift correction:* The bead positions were tracked over time to generate a drift list file containing the central x, y coordinates of AOIs as a function of time (number of frames); see Figure S3. (3) *Identification of protein landings on vesicles:* The criteria used for the start of a protein landing on a vesicle were that the intensity of an AOI (spot) in the protein channel must be above the user-determined noise level and the center of the same AOI must be less than 3 pixels from the center of a vesicle AOI. The initial detection is performed after the user defines the characteristic noise diameter, spot diameter and spot intensity as previously described.[7] Landings (events) ended when the protein AOI was 4.5 pixels or more away from the center of the vesicle AOI (or had disappeared entirely).

In the absence of vesicles, no long-lived, longer than 30 ms (one frame), protein landings were observed.

Residence Time Analysis

Three datasets were collected using 488 nm laser powers of 4, 8 or 10 mW, measured before the objective. The datasets contained 309, 5085 and 405 individual residence times, respectively (Fig. S4). The dissociation rate constant, k_{off}, was determined from the raw residence times by fitting to a single exponential (Equation 1 in the main text) using maximum likelihood methods implemented in Matlab. Fits to a double exponential did not improve the quality of the fits. The uncertainty in k_{off} was determined from the standard deviation of 5000 bootstraps for each dataset. Probability distribution functions (pdfs) were determined by binning the data using 0.03 s (minimum time resolution) bins for short residence times and larger binning times for longer residence times where fewer events were detected (≤0.45 s for the smaller 4 and 10 mW datasets and ≤0.99 s for the larger 8 mW dataset). The number of events in each bin was divided by the total number of events in the dataset and the time width of the bin to generate the final pdf (Fig. S4).

The effect of photobleaching on the apparent k_{off} was determined from a weighted linear fit to the apparent k_{off} versus laser power (Fig. S4) performed in Matlab using the equation:

$$k_{off} = k_o + Pk_{bleach} \qquad \text{(S1)}$$

where k_o is the dissociation rate constant, k_{bleach} is the power-dependent contribution of photobleaching to the apparent k_{off} and P is the laser power. The weights for the fits were the standard deviations, σ,

determined for k_{off} at each power from the maximum likelihood fits to the residence time data. This resulted in significantly more weight for the ~10 times larger 8 mW data set ($\sigma = 0.053\ s^{-1}$) than for the smaller 4 mW ($\sigma = 0.19\ s^{-1}$) and 10 mW ($\sigma = 0.20\ s^{-1}$) datasets. Uncertainties for the fitting parameters k_o and k_{bleach} were determined by bootstrapping using Gaussian pdfs defined by k_{off} from the maximum likelihood fits and the standard deviation for each power, σ.

Determining Vesicle Intensities

Vesicles photobleached faster if excited by both the 647 and 488 nm lasers. Therefore, vesicle intensities were determined from the first 5 frames (150 msec) obtained for each field of view collected before turning on the 488 nm excitation. The average intensity of SUVs containing a single DiD, 1000 a.u., was determined from separate vesicle photobleaching experiments, using only 647 nm excitation, by averaging the intensity of the last step in SUV photobleaching traces. In Figure 2D, the bin size for the vesicle intensity is the average intensity for SUVs containing only a single DiD molecule, i.e., 1000 a.u.

Molecular Dynamics (MD) Simulations

Preparation of the Lipid Bilayer

The DMPC:DMPG (1,2-dimristoyl-*sn*-glycero-3-phosphocholine:1,2-dimristoyl-*sn*-glycero-3-phospho-(1'-rac-glycerol)) mixed bilayer (80:20, X_{PC}=0.8) containing 256 lipids (204 DMPC and 52 DMPG lipids) evenly distributed between the two leaflets was constructed using the CHARMM-GUI[8]. A total of 9242 TIP3P[9,10] water molecules were added to hydrate the lipids, and lastly 52 sodium ions were randomly added to achieve an overall neutral system. The CHARMM36 force field[11] and NAMD (v2.9)[12] were used for the simulations. The bilayer was first minimized using 4000 steps of a conjugate gradients algorithm. The system was then equilibrated at 310 K, and 1 atm in the NPT ensemble for 400 ps with constant area in the x-y dimension and 2 fs time steps. The temperature was controlled with Langevin dynamics with the temperature damping coefficient set to 1.0 and the velocities were periodically reassigned every 1 ps. The pressure was controlled using the Langevin piston method[13] with an oscillation period of 75 fs and a damping time scale of 25 fs. Anisotropic pressure coupling was used. The nonbonded interactions cut-off was set to 12 Å and long-range electrostatics corrections beyond the cut-off were added using the Particle Mesh Ewald[14] method. We used switching functions for both the electrostatics and van der Waals interactions with the switch distance set to 11 Å. We used the r-RESPA[15] multiple time step algorithm and short-range non-bonded forces were evaluated every 2 fs while long-range electrostatics were evaluated every 4 fs. SHAKE[16] was used to constrain all bonds between hydrogen atoms and heavy atoms. The system was then further equilibrated for 200 ps after removing the constant area constraint.

The bilayer system was further equilibrated for 100 ns in the NPT ensemble using anisotropic pressure coupling and no velocity reassignment. The pressure control parameters for the Langevin piston method were altered to 200 fs for the oscillation period and 50 fs for the damping time scale. All other simulation parameters remained unchanged. The resulting area per lipid was 59.6 ± 0.9 $Å^2$.

Initial Protein Docking

The structure of wild-type *Bt*PI-PLC, an overall anionic protein with a net charge of -7, was constructed as described by Grauffel et al.[17] The starting orientation of membrane bound *Bt*PI-PLC was obtained from implicit membrane simulations.[17] The protein was then manually docked on the pre-equilibrated mixed bilayer. Four lipids (three DMPC and one DMPG) were removed to avoid coordinate

overlapping and steric clashes. Then the system was minimized as described by Grauffel et al.[17] and solvated with TIP3P water molecules using VMD[18]. After solvation, six additional sodium ions were added by randomly replacing water molecules to achieve an overall charge neutral system.

*Bt*PI-PLC and Lipid MD Simulations

The combined lipid-protein system was then subjected to two short 400 ps equilibrations in the NVT ensemble with constraints on the protein backbone. Subsequently, the system was equilibrated for 2 ns in the NPT ensemble without any constraints before finally performing the 500 ns NPT simulation. The temperature was set to 310 K during the simulation with a 2 fs integration time step in NAMD (v2.9).[12] The temperature was controlled as described above for the mixed bilayer. The pressure was set to 1 atm with an oscillation period of 200 fs and a damping time scale of 50 fs. The CHARMM all-atom force field (c22 including CMAP correction)[10, 19] and the force field update for lipids (CHARMM36)[11] were used. Trajectory conformations were saved every 10 ps.

Two simulations were performed with different initial positions of *Bt*PI-PLC relative to the lipid bilayer. In the second replicate, the protein was rotated by 180 degrees around the bilayer normal (z-axis) to allow for different initial protein-lipid contacts. This was done to avoid bias in protein-lipid interactions due to the initial distribution of lipids under or around the protein. The first simulation, *MD replica 1,* is 500 ns long and the second, *MD replica 2,* is 497.5 ns long. The similarities between the results of the two independent trajectories, as previously observed for similar time scale simulations performed using different lipid compositions,[17] provides evidence that the simulations have reached an equilibrium.

Trajectory Analysis

All analyses were performed using CHARMM (v33b1)[20] and VMD (v1.9.1)[18] on the last 450 ns of each simulation.

Hydrophobic interactions between the protein and lipid bilayer were assigned if the protein and membrane candidate atoms were within 3 Å of each other for at least 10 ps. For the protein, candidate atoms for hydrophobic contacts are side chain atoms from aliphatic groups, while for the lipid bilayer, the candidate atoms are those from the hydrophobic lipid tails. Hydrogen bonds were assigned using the donor and acceptor definitions from the CHARMM[10] force field with a distance cut-off of 2.4 Å and an angle cut-off of 130 degrees. The two cut-off criteria had to be met for at least 10 ps. We used two criteria to identify cation-π adducts between the aromatic amino acids (Tyr, Phe and Trp) and the choline group of the DMPC lipids: (i) the nitrogen atom of the choline group should be within 7 Å of each atom of the aromatic rings and (ii) these distances should not vary by more than 1.5 Å.[17]

Occupancy of a particular interaction was calculated as the number of conformations with the interaction present divided by the total number of conformations in the trajectory sampling window (Figures 4 and S8).

Electron density profiles (EDP) were generated using the Density Profile Tool[21] VMD plugin. EDPs were calculated from the trajectories at 1 ns intervals. The projection axis is the z-axis, which is also the bilayer normal. The profile resolution is $\Delta z = 1$ Å for the protein, lipid bilayer and water. The profile resolution is $\Delta z = 0.5$ Å for amino acids, membrane binding components of protein, choline and phosphate planes of the membrane.

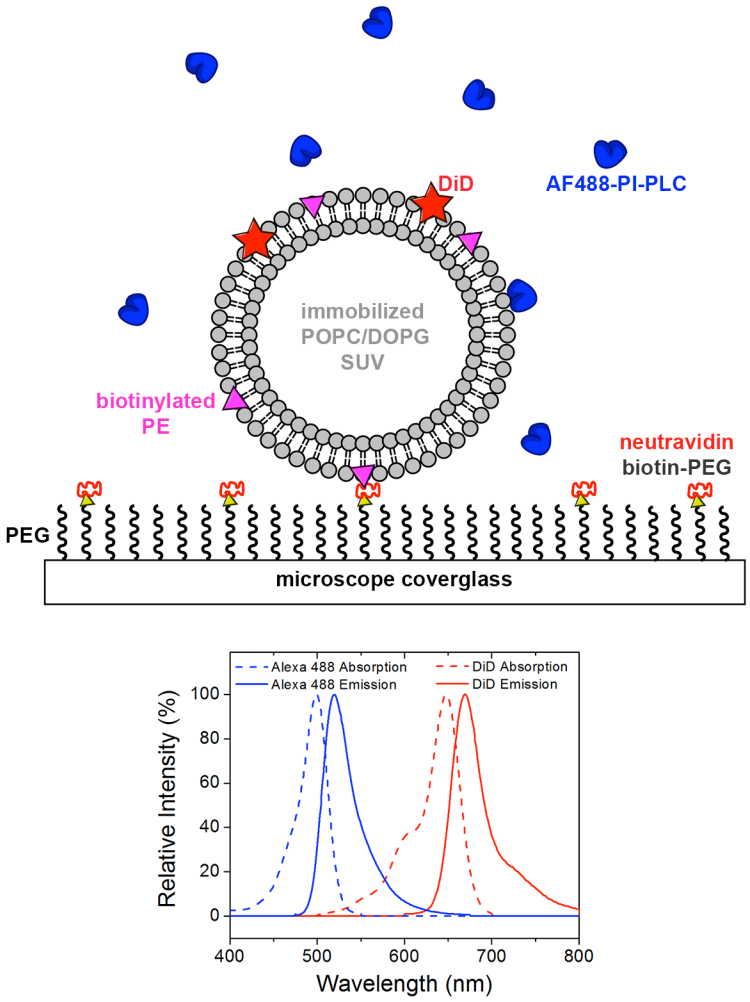

Figure S1. Sample schematic showing vesicle immobilization. (A) SUVs containing biotin-PE are immobilized via neutravidin on a PEG surface containing 1% biotin-PEG. (B) The emission of AF488 labeled *Bt*PI-PLC (solid blue lines) and SUVs containing DiD (solid red lines) are spectrally distinct allowing us to image using a dual-view microscopy setup with a single camera[6] that separates the two channels at 630 nm. This insures simultaneous observation of AF488 labeled *Bt*PI-PLC and DiD labeled SUVs in the single molecule TIRF experiments.

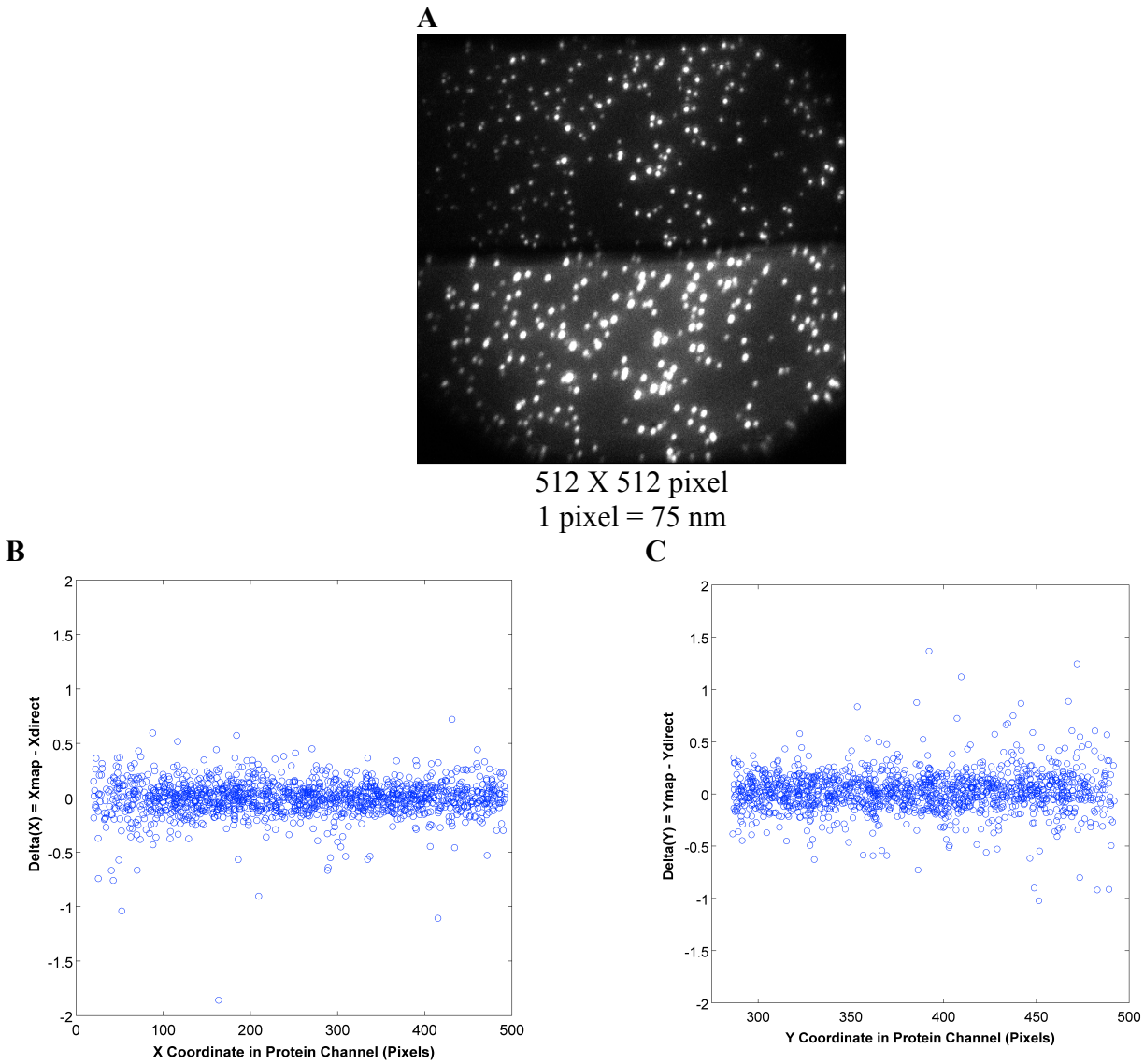

Figure S2. Image analysis showing the efficacy of mapping between the <630 nm and >630 nm channels. Fluorescent beads which can be imaged in both channels were used to determine illumination uniformity, to generate mapping files, as described in the methods above and by Friedman, Mumm and Gelles,[7] and for drift correction for each day of experiments. (A) Fluorescence images of individual beads in both the <630 nm (protein, upper) and >630 nm (vesicle, lower) channels. Due to the non-uniformity of illumination at the edges, only the central region was used for detecting landings of proteins and extracting intensities of fluorescently labeled vesicles. Over 1000 bead images were used to generate the data for mapping the x and y coordinates from the vesicle channel to the protein channel. This mapping was used when analyzing vesicle binding data collected on the same day. The accuracy of the mapping algorithm is within one pixel as shown by: (B) Delta(X), the difference between the x-coordinate determined by mapping from the vesicle into the protein channel (Xmap) and the position determined directly from Gaussian fits to the bead images in the protein channel (Xdirect), vs. Xdirect. (C) Delta(Y) vs. Ydirect.

A

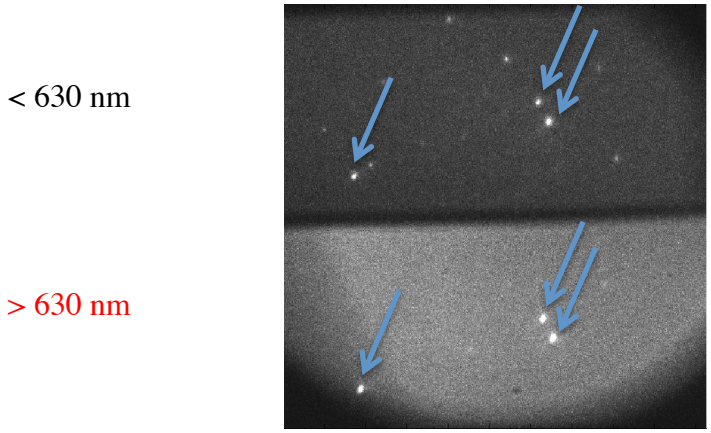

B

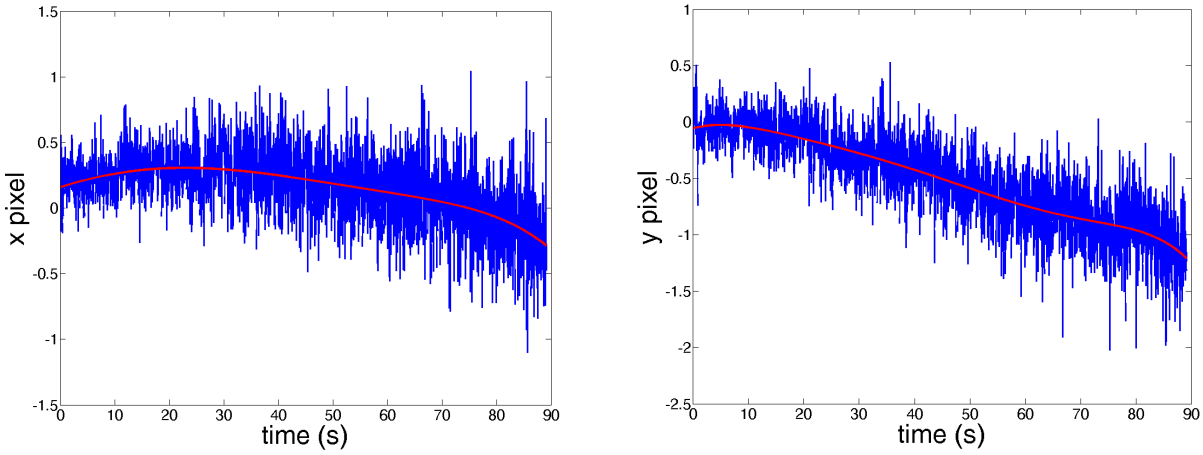

Figure S3. Drift correction from bead images. (A) One frame (30 ms exposure time) from a movie in which both the 647 nm and 488 nm lasers were on for 10 s. Fluorescent beads are indicated by arrows, DiD labeled vesicles (> 630 nm) have photobleached, and several landings of AF488 labeled *Bt*PI-PLC (< 630 nm) were observed in the < 630nm channel. (B) The bead positions as a function of time (left: x and right: y) during the movie (blue). The third order polynomial fit, used to correct the protein and vesicle positions over time, is shown in red.

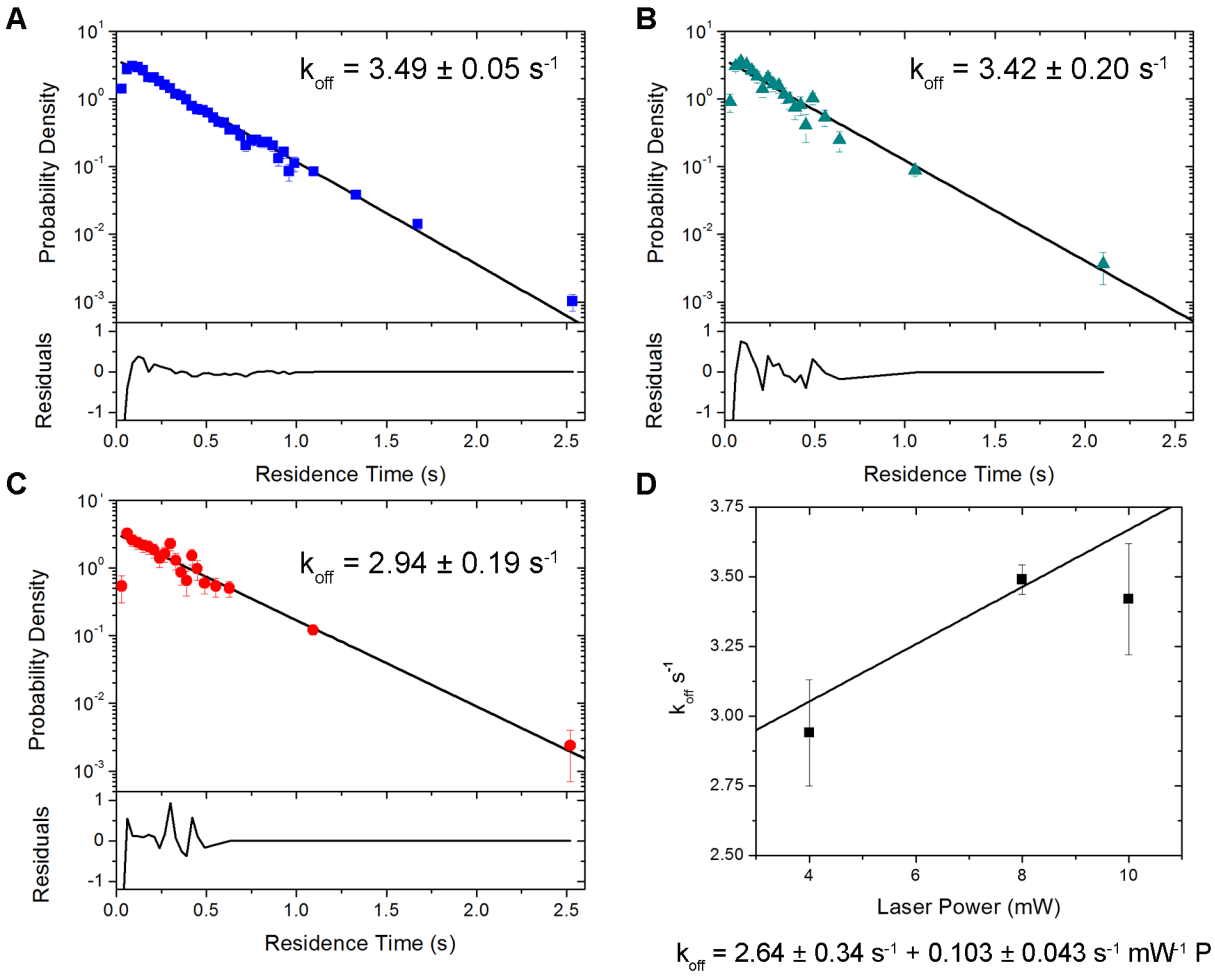

Figure S4. Determining k_{off}. Probability distribution functions (pdf) for *Bt*PI-PLC residence times on POPC/DOPG SUVs compared to the pdfs determined from maximum likelihood fits for different laser powers. The lines are the pdfs using k_{off} from the maximum likelihood fits to the raw data and the points are the experimental pdfs for different laser powers: (A) 8 mW, 5085 events, (B) 10 mW, 405 events & (C) 4 mW, 309 events. The error bars, w_i, were determined assuming that the probability of observing n_i events in the ith bin of the pdf are binomially distributed:

$$w_i = \frac{\sqrt{\frac{n_i}{N}\left(1-\frac{n_i}{N}\right)}}{N\ t_{bin,i}}$$

where N is the total number of events (residence times), n_i/N is the probability of observing n_i events in a bin and $t_{bin,i}$ is the time per bin. The residuals, the difference between the pdf determined from the experimental data and the pdf determined from the maximum likelihood fits to the raw data, are also plotted for each laser power. The residuals for the first, 0 to 0.03 s, bin are off-scale due to the limited time resolution (see the main text). (D) To determine k_{off} in the absence of photobleaching, k_o, the dissociation rate constants determined for 4, 8 and 10 mW (panels A-C) were fit to Equation S1 (line) yielding $k_o = 2.64 \pm 0.34\ s^{-1}$ and a power dependence of $k_{bleach} = 0.103 \pm 0.043\ mW^{-1}\ s^{-1}$ where the uncertainties were determined by bootstrapping. The error bars for k_{off} correspond to the standard deviations of the maximum likelihood fits (shown in A-C) and these standard deviations were used as weights in the linear fit.

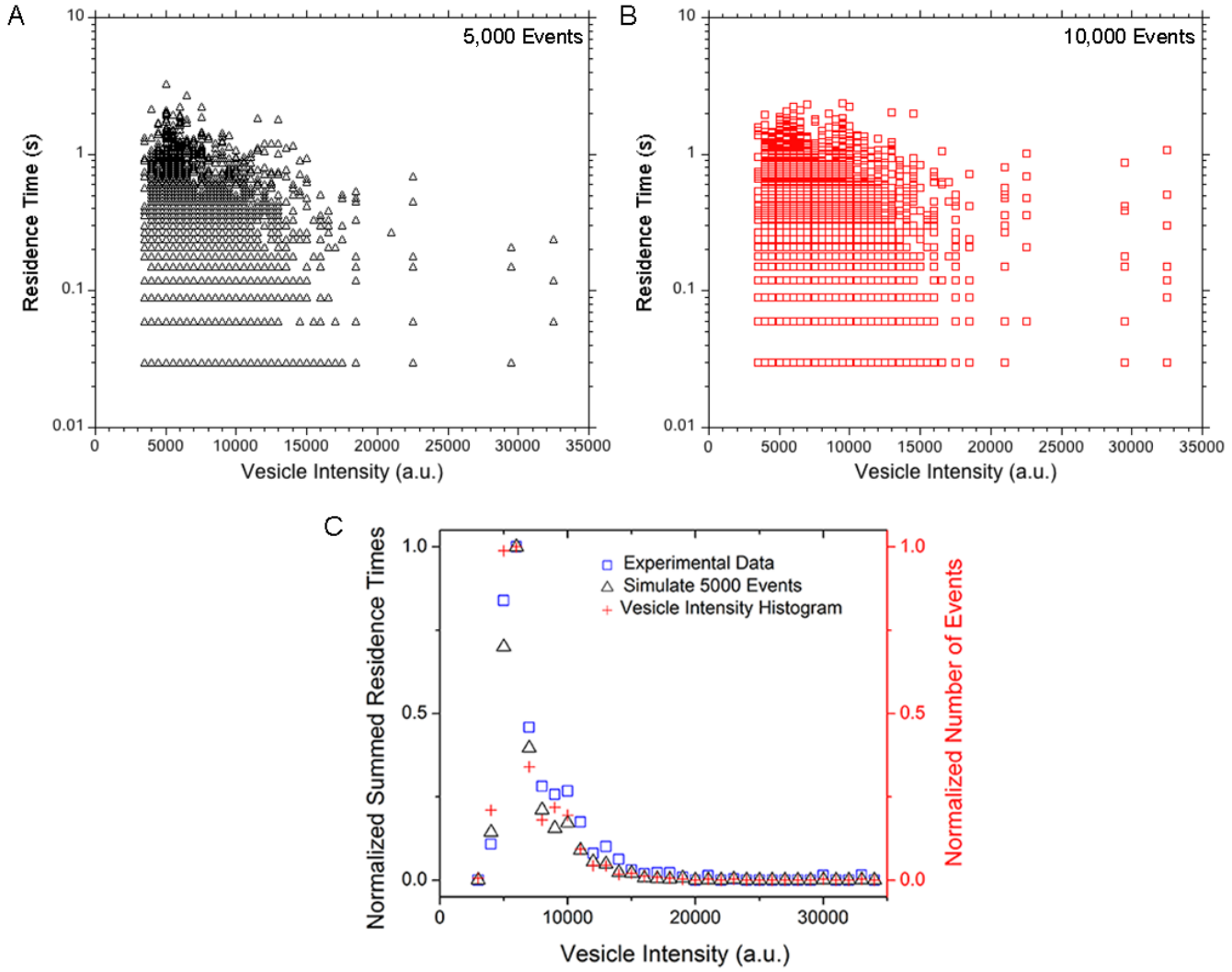

Figure S5. Predicted plots of protein residence time versus vesicle fluorescence intensity in the absence of vesicle size dependence. (A) These plots were generated by randomly picking (A) 5,000 or (B) 10,000 data points from the probability distributions for protein residence time and vesicle intensity (size). Note that doubling the number of points does not significantly change the distribution indicating that 5,000 points, as determined from the TIRF experiments (488 nm laser power = 8mW), are sufficient to define the distribution. (C) The size independence of the residence times is further supported by plotting the summed residence times versus vesicle intensity (size). Both the experimental data from TIRF experiments (blue squares) and the simulated data (black triangles) show similar distributions. Furthermore, the distribution of the summed residence times versus vesicle intensity (size) is similar to the distribution of vesicle size (crosses) from the measured vesicle intensities, which also suggests that protein residence times are independent of vesicle size.

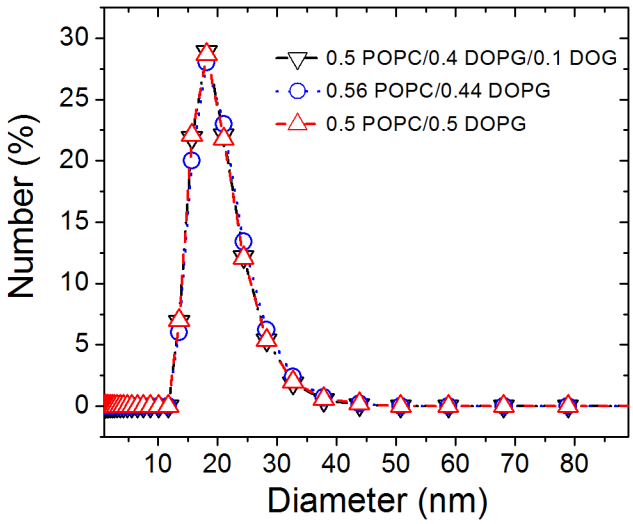

Figure S6. SUVs with different lipid compositions have similar size distributions. Size distributions of lipid vesicles with different lipid compositions were measured by dynamic light scattering using a Malvern Nano Zetasizer. The SUV lipid composition is indicated in the legend.

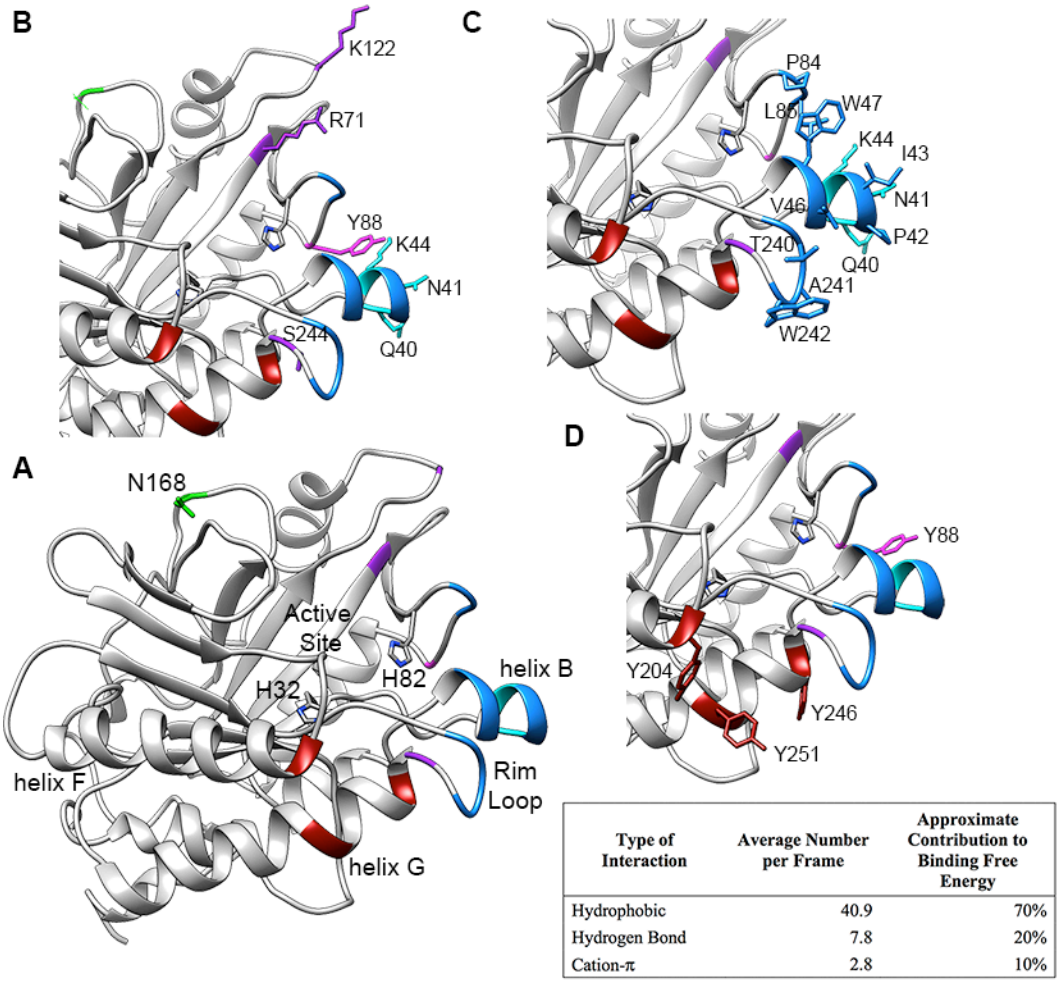

Type of Interaction	Average Number per Frame	Approximate Contribution to Binding Free Energy
Hydrophobic	40.9	70%
Hydrogen Bond	7.8	20%
Cation-π	2.8	10%

Figure S7. The *Bacillus* PI-PLC membrane binding interface. (A) A snapshot of the *Bt*PI-PLC structure from the protein-membrane MD simulations with the membrane binding interface to the right. PI-PLC is a member of the TIM barrel superfamily. The active site for cleavage of PI and GPI is in the β barrel and is indicated by His32 and His82. Residues that make large energetic contributions to membrane binding, based on data from experiments[1,17,22,23] and MD simulations[17], are colored according to how they interact with the lipid bilayer: blue: hydrophobic interactions; cyan: hydrophobic and hydrogen bond interactions; purple: hydrogen bond interactions; magenta: hydrogen bond interactions and cation-π interactions and red: cation-π interactions with choline headgroups. The site for fluorescent labeling (N168C) is shown in green. (B) A more detailed view of the residues involved in hydrogen bonding interactions with the membrane. (C) A more detailed view of the residues involved in hydrophobic interactions with the membrane. (D) A more detailed view of the residues involved in cation-π interactions with choline headgroups. The table lists the average number of each type of interaction observed per frame in the MD simulations. These protein structure figures were generated using UCSF Chimera.[24]

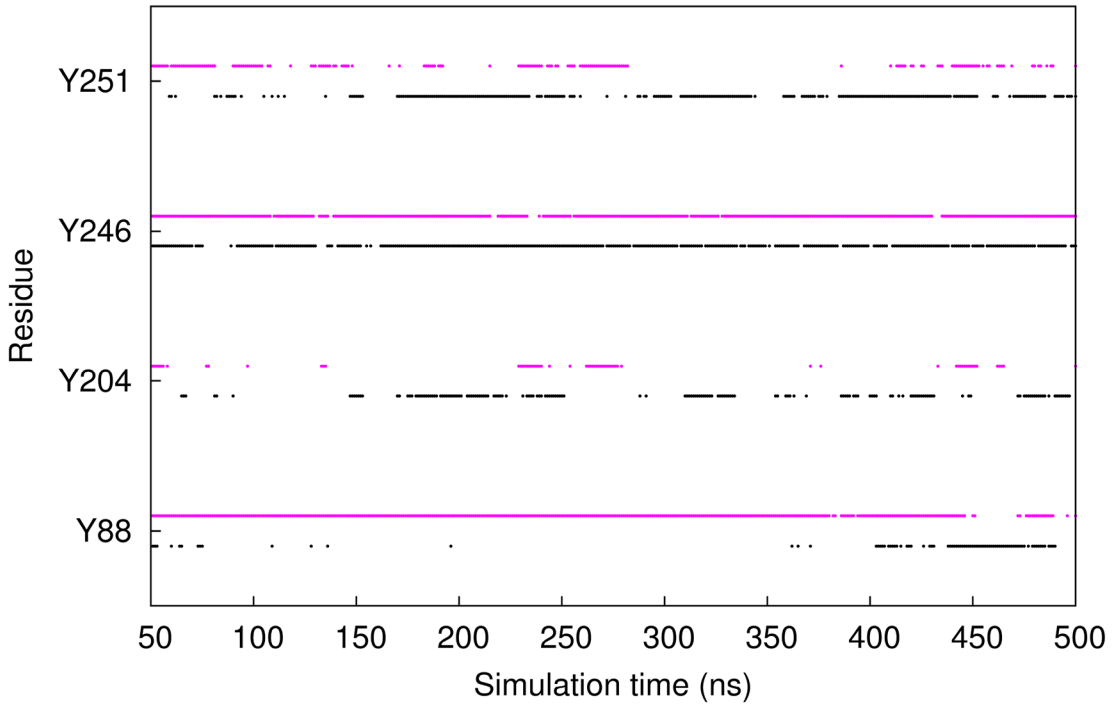

Figure S8. Occupancies of important protein-lipid cation-π interactions during the simulations. Cation-π interactions of Tyr residues with choline headgroups of DMPC lipids (black dots for MD replica one and magenta dots for MD replica two). These Tyr residues were identified as having the highest contributions to vesicle binding by combining experimental binding data and MD simulations for *Bt*PI-PLC variants including wild-type.[17]

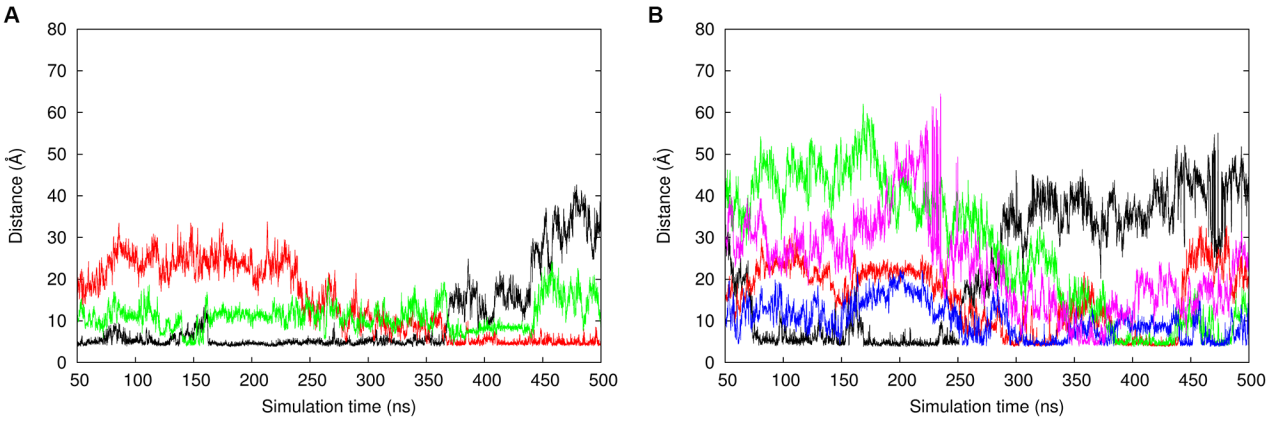

Residue	Replica 1	Replica 2
Y251	13	11
Y246	5	3
Y204	9	7
Y88	6	3

Figure S9. Transient nature of cation-π interactions as multiple lipids engage with Tyr residues. (A) Distance between the center of mass of the Tyr246 aromatic ring and the nitrogen atom in DMPC choline headgroups (replica one). Each color represents a distinct DMPC lipid. Lipids with cation-π occupancies below 2.5% are not shown. (B) Same as A, but for Tyr251. Lipids with cation-π occupancies below 4% are not shown. The number of DMPC lipids mediating cation-π interactions are tabulated at the bottom.

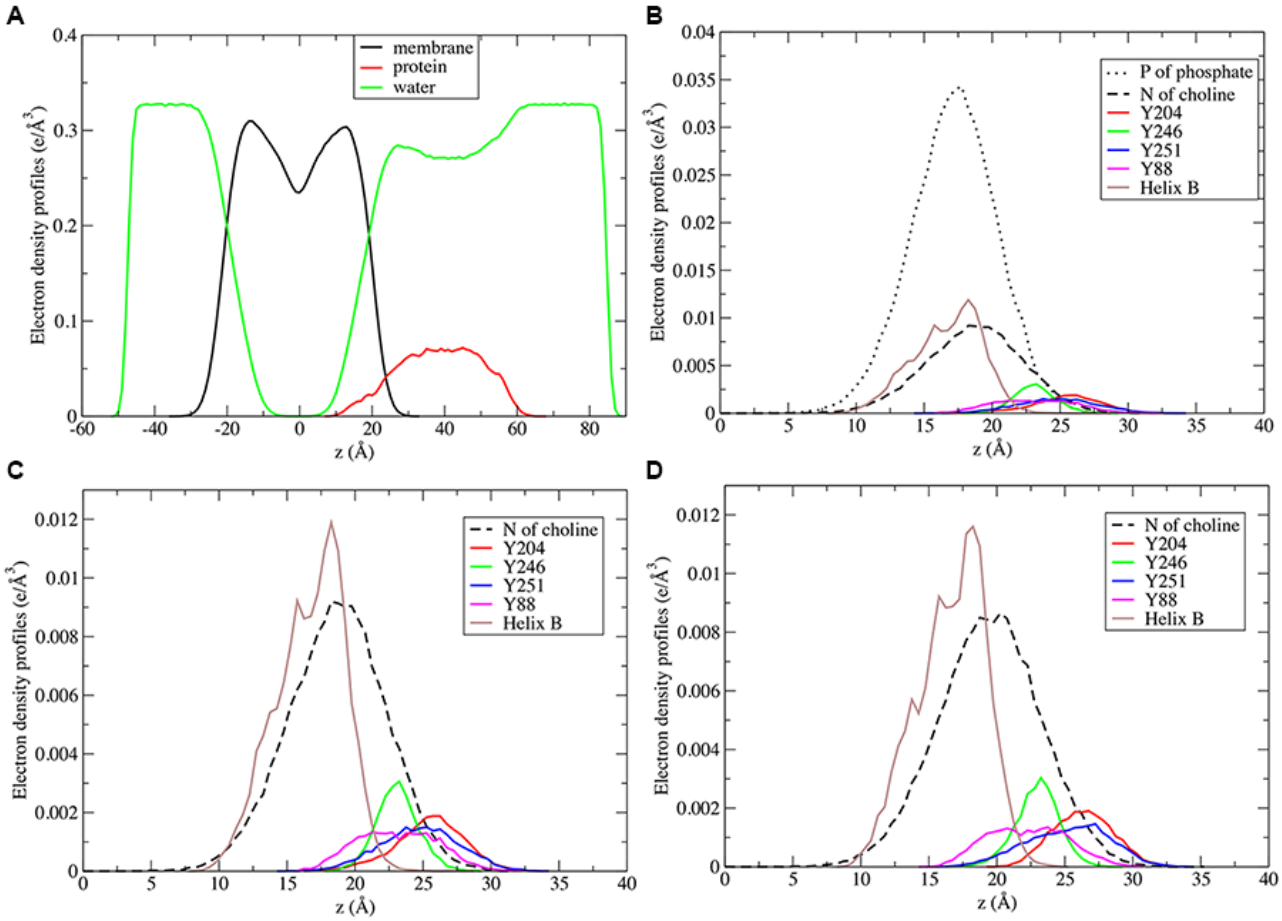

Figure S10. Residues from *Bt*PI-PLC that interact with the membrane are located near the membrane surface. Electron density profiles from the MD simulations (except as noted all graphs are from MD simulation replica one). The center of the lipid bilayer is defined as 0 Å. (A) *Bt*PI-PLC is localized just above the membrane surface. (B) Localization of *Bt*PI-PLC Tyr residues and helix B in the upper leaflet relative to the plane defined by the lipid phosphates and the plane defined by the choline headgroups. Helix B, which mediates significant hydrophobic interactions, is more deeply inserted than the Tyr residues, which are located mostly at the membrane-water interface. (C) Helix B has at least two preferred positions (brown curve), with the most populated one around 18 Å from the center of the bilayer. By contrast, Tyr246 is located around 23 Å from the bilayer center whereas Tyr88 shows a broader range of expected positions, between 21 and 25 Å from the bilayer center. The most probable locations of these Tyr residues significantly overlap with the choline distributions. Tyr residues 204 and 251 are located closer to the membrane surface with expected positions of around 26 Å and between 23 and 26 Å from the center of the bilayer, respectively. These two residues show less overlap with the choline distributions. (D) Same as (C) only from MD simulation replica two. In this simulation, the Tyr residues, particularly Tyr88, have a slightly larger overlap with the choline distributions.

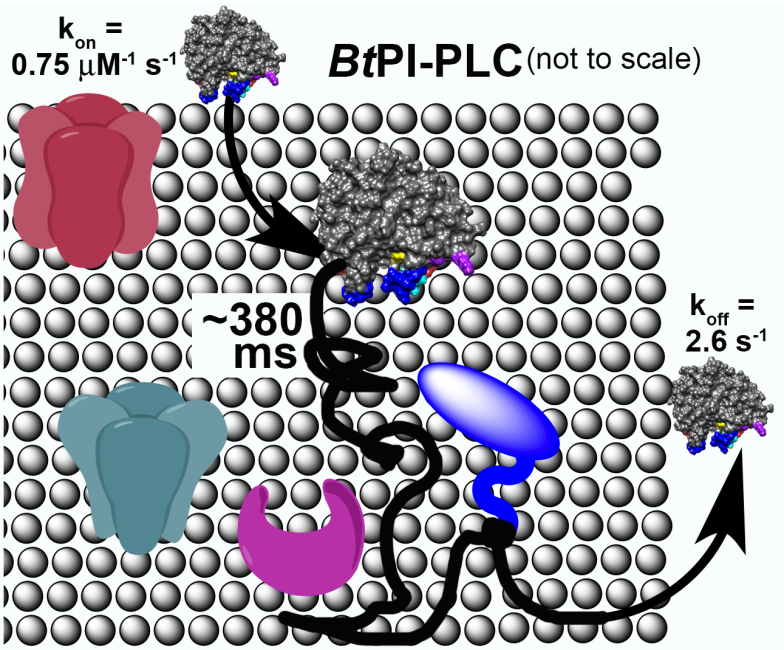

Figure S11. A schematic of the proposed *Bt*PI-PLC membrane search mechanism, looking down on the membrane. *Bt*PI-PLC (spacefill) is colored as depicted in Figure 4B, with residues that interact with the membrane colored blue, purple and red indicating hydrophobic, hydrogen bonding and cation-π interactions with the membrane, respectively. The membrane and integral membrane proteins are shown schematically.

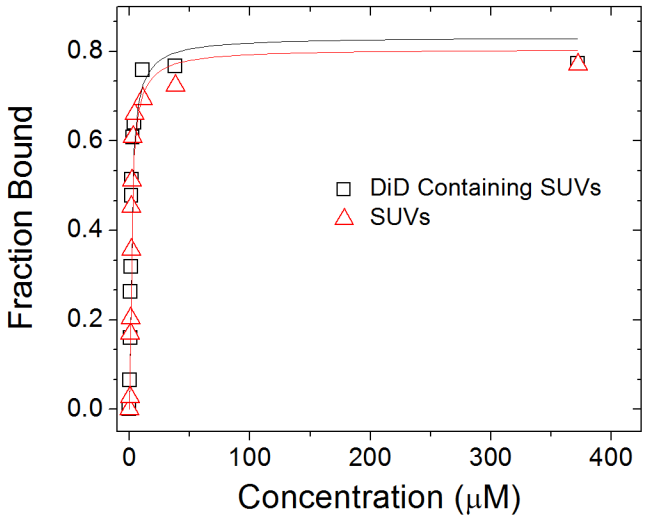

Figure S12. DiD incorporation does not significantly alter *Bt*PI-PLC binding. Binding curves, determined by FCS for AF488 lableled *Bt*PI-PLC binding to 0.8/0.2 mole fraction POPC/DOPG SUVs with (black squares) and without (red triangles) 3 mole percent DiD.

References:

(1) Feng, J.; Wehbi, H.; Roberts, M. F. *J. Biol. Chem.* **2002**, *277*, 19867.

(2) Pu, M.; Fang, X.; Redfield, A. G.; Gershenson, A.; Roberts, M. F. *J. Biol. Chem.* **2009**, *284*, 16099.

(3) Cheng, J.; Goldstein, R.; Stec, B.; Gershenson, A.; Roberts, M. F. *J. Biol. Chem.* **2012**, *287*, 40317.

(4) Englander, S. W.; Calhoun, D. B.; Englander, J. J. *Anal. Biochem.* **1987**, *161*, 300.

(5) Ha, T. *Methods* **2001**, *25*, 78.

(6) Kinosita, K.; Itoh, H.; Ishiwata, S.; Hirano, K.; Nishizaka, T.; Hayakawa, T. *J. Cell Biol.* **1991**, *115*, 67.

(7) Friedman, L. J.; Mumm, J. P.; Gelles, J. *Proc. Natl. Acad. Sci. U. S. A.* **2013**, *110*, 9740.

(8) Jo, S.; Kim, T.; Iyer, V. G.; Im, W. *J. Comput. Chem.* **2008**, *29*, 1859.

(9) Jorgensen, W. L.; Chandrasekhar, J.; Madura, J. D.; Impey, R. W.; Klein, M. L. *J. Chem. Phys.***1983**, *79*, 926.

(10) MacKerell, A. D.; Bashford, D.; Bellott; Dunbrack, R. L.; Evanseck, J. D.; Field, M. J.; Fischer, S.; Gao, J.; Guo, H.; Ha, S.; Joseph-McCarthy, D.; Kuchnir, L.; Kuczera, K.; Lau, F. T. K.; Mattos, C.; Michnick, S.; Ngo, T.; Nguyen, D. T.; Prodhom, B.; Reiher, W. E.; Roux, B.; Schlenkrich, M.; Smith, J. C.; Stote, R.; Straub, J.; Watanabe, M.; Wiórkiewicz-Kuczera, J.; Yin, D.; Karplus, M. *J. Phys. Chem. B* **1998**, *102*, 3586.

(11) Klauda, J. B.; Venable, R. M.; Freites, J. A.; O'Connor, J. W.; Tobias, D. J.; Mondragon-Ramirez, C.; Vorobyov, I.; MacKerell, A. D.; Pastor, R. W. *J. Phys. Chem. B* **2010**, *114*, 7830.

(12) Kalé, L.; Skeel, R.; Bhandarkar, M.; Brunner, R.; Gursoy, A.; Krawetz, N.; Phillips, J.; Shinozaki, A.; Varadarajan, K.; Schulten, K. *J. Comput. Phys.* **1999**, *151*, 283.

(13) Feller, S. E.; Zhang, Y.; Pastor, R. W.; Brooks, B. R. *J. Chem. Phys.* **1995**, *103*, 4613.

(14) Essmann, U.; Perera, L.; Berkowitz, M. L.; Darden, T.; Lee, H.; Pedersen, L. G. *J. Chem. Phys.* **1995**, *103*, 8577.

(15) Izaguirre, J. s. A.; Reich, S.; Skeel, R. D. *J. Chem. Phys.* **1999**, *110*, 9853.

(16) Andersen, H. C. *J. Comput. Phys.* **1983**, *52*, 24.

(17) Grauffel, C.; Yang, B.; He, T.; Roberts, M. F.; Gershenson, A.; Reuter, N. *J. Am. Chem. Soc.* **2013**, *135*, 5740.

(18) Humphrey, W.; Dalke, A.; Schulten, K. *J. Mol. Graphics* **1996**, *14*, 33.

(19) Mackerell, A. D.; Feig, M.; Brooks, C. L. *J. Comput. Chem.* **2004**, *25*, 1400.

(20) Brooks, B. R.; Brooks, C. L.; Mackerell, A. D.; Nilsson, L.; Petrella, R. J.; Roux, B.; Won, Y.; Archontis, G.; Bartels, C.; Boresch, S.; Caflisch, A.; Caves, L.; Cui, Q.; Dinner, A. R.; Feig, M.; Fischer, S.; Gao, J.; Hodoscek, M.; Im, W.; Kuczera, K.; Lazaridis, T.; Ma, J.; Ovchinnikov, V.; Paci, E.; Pastor, R. W.; Post, C. B.; Pu, J. Z.; Schaefer, M.; Tidor, B.; Venable, R. M.; Woodcock, H. L.; Wu, X.; Yang, W.; York, D. M.; Karplus, M. *J. Comput. Chem.* **2009**, *30*, 1545.

(21) Giorgino, T. *Comput. Phys. Commun.* **2014**, *185*, 317.

(22) Pu, M.; Orr, A.; Redfield, A. G.; Roberts, M. F. *J. Biol. Chem.* **2010**, *285*, 26916.

(23) Pu, M.; Roberts, M. F.; Gershenson, A. *Biochemistry* **2009**, *48*, 6835.

(24) Pettersen, E.; Goddard, T.; Huang, C.; Couch, G.; Greenblatt, D.; Meng, E.; Ferrin, T. *J. Comput. Chem.* **2004**, *25*, 1605.